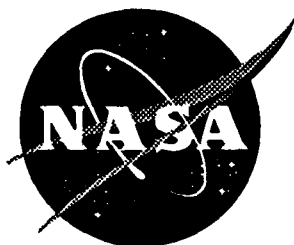NASA Technical Memorandum 109127

41 P

Kinematic Modeling of a Double Octahedral Variable Geometry Truss (VGT) as an Extensible Gimbal

Robert L. Williams II
Langley Research Center, Hampton, Virginia

May 1994

Kinematic Modeling of a Double Octahedral
Variable Geometry Truss (VGT) as an Extensible Gimbal

Robert L. Williams II

ABSTRACT

This paper presents the complete forward and inverse kinematics solutions for control of the three degree-of-freedom (DOF) double octahedral variable geometry truss (VGT) module as an extensible gimbal. A VGT is a truss structure partially comprised of linearly actuated members. A VGT can be used as joints in a large, lightweight, high load-bearing manipulator for earth- and space-based remote operations, plus industrial applications . The results have been used to control the NASA VGT hardware as an extensible gimbal, demonstrating the capability of this device to be a joint in a VGT-based manipulator. This work is an integral part of a VGT-based manipulator design, simulation, and control tool.

1. INTRODUCTION

Variable geometry trusses (VGTs) are a class of in-parallel actuated devices. In-parallel actuated manipulators have several load paths from the end-effector to the fixed link, as opposed to serial manipulators which have only one. They are truss structures with linear actuators for some members. VGTs retain the desired stiffness and load-bearing characteristics of trusses, while providing the capability to articulate. VGT manipulators are lightweight, have long reach, and are high load bearing compared to equivalent serial manipulators. All actuators are linear, which are preferable to rotary joints. VGT manipulators can be constructed in a modular fashion, allowing many redundant degrees of freedom (DOF). This redundancy can be used to optimize performance, such as providing snake-like motion to avoid obstacles, avoiding singularities, and avoiding joint limits. The VGT has an open structure allowing routing of cables and hoses. When properly designed, all VGT members are loaded axially, thus increasing stiffness and load bearing capability.

The double octahedral VGT (Fig. 1) was developed at NASA Langley in the 80's (Rhodes and Mikulas, 1985). It was intended to be used in large deployable space structures. VGTs were then pursued as active structural elements to damp vibrations of large space structures (Wynn and Robertshaw, 1991). Recently, researchers have considered using VGTs as robotic manipulators (Millsap, et. al., 1992). These authors propose a large-scale VGT-based manipulator to clean up large waste storage tanks. The Department of Energy (DOE) determined that the state of the art in large manipulators was not sufficient to efficiently handle this problem (Millsap, et. al., 1992). Another DOE application for VGT technology is as a trunk for carrying two dexterous serial manipulators on a decontamination and decommissioning vehicle for cleaning up contaminated nuclear facilities, under development at Oak Ridge National Laboratories.

The VGT shown in Fig. 1 has three DOF. It can be used as a joint in a modular manipulator constructed of articulating joints and static truss sections. In this paradigm, it is convenient to control the VGT module as a gimbal, with α, β rotations about perpendicular axes. In addition, accordion-like extension of the VGT joint is possible. This extension can be fixed at a nominal middle value (i.e. constrain the three DOF to two). However, to obtain the most capability, all three DOF should be coordinated. The purpose of the current paper is to present the complete forward and inverse position kinematic solutions to control the double octahedral VGT (hereafter referred to as VGT) as an extensible gimbal.

The groundbreaking theoretical kinematics work for this VGT was performed at Virginia Polytechnic Institute & State University. Padmanabhan (1992) presents a general study of VGTs (called isostatic frameworks) in his PhD dissertation. The double octahedral VGT is a case study in this work. Padmanabhan, Tidwell, Salerno, and Reinholtz (1992) present the concept and general solutions for using the VGT as a gimbal. Padmanabhan, Arun, and Reinholtz (1990) present a general closed-form solution to the VGT inverse position problem.

The primary contribution of the present paper is that it summarizes all kinematics equations necessary to model the VGT as an extensible gimbal, including full details. Original work reported includes formalization of the subproblems for forward and inverse position kinematics, Stewart platform analogy for the forward solution, closed-form expressions for the improvement vector at each Newton-Raphson iteration for the forward solution, VGT mobility calculation, VGT node locations calculation, and presentation of the complete forward transformation for the extensible gimbal.

The current paper is organized as follows. Section 2 summarizes the symbols used throughout the paper. Section 3 presents the paradigm for controlling the VGT as an extensible gimbal. Section 4 presents the complete forward and inverse position kinematics solutions for the VGT, including the extensible gimbal equations. Section 5 gives examples to demonstrate the various solutions. Appendix A presents mobility calculations for the VGT, Appendix B presents fixed VGT geometry, Appendix C applies the Newton-Raphson method to the VGT forward kinematics solution, Appendix D provides extensible gimbal details, and Appendix E presents a method to calculate the VGT node locations for finite element modeling and general simulation.
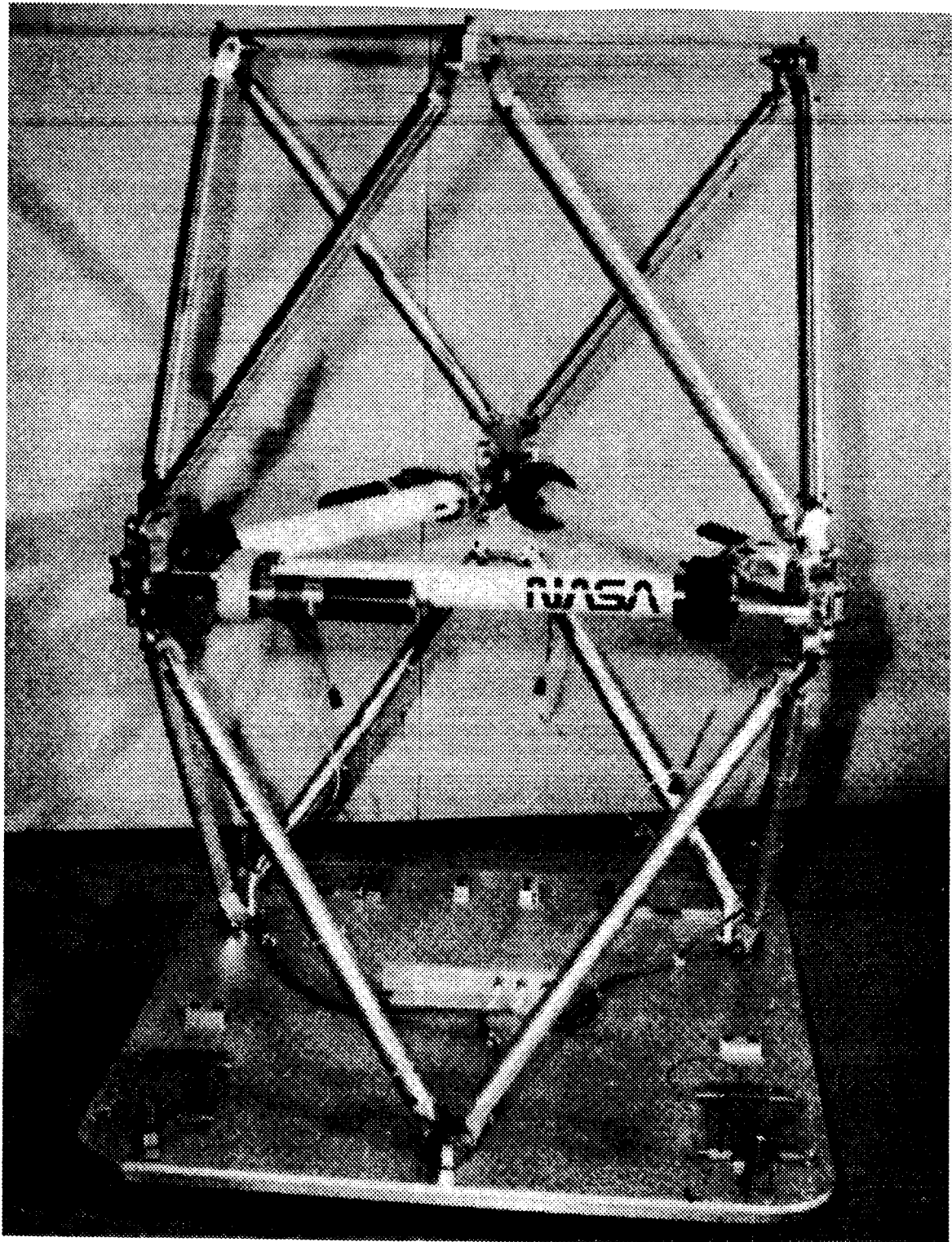
Figure 1
NASA VGT Hardware

2. SYMBOLS

$a_i; i = 1,2,3$ — Vectors locating $Q_i; i = 1,2,3$ in actuation plane

A, B, C, D, E — Simplified forward kinematics coefficients

B_1, B_2, B_3 — Base nodes

B_{1R}, B_{2R}, B_{3R} — Top platform nodes

$\{B\}, \{P\}$ — Base and platform coordinate frames

c_i, s_i — $\cos\theta_i$, $\sin\theta_i$

$D_i, E_i, F_i; i = 1,2,3$ — Forward kinematics coefficients

$E_i, F_i, G_i; i = 1,2,3$ — Inverse kinematics coefficients

L — Cross longeron length

L_0 — Fixed batten length

L_1, L_2, L_3 — VGT input leg lengths

L_{MIN}, L_{MAX} — Minimum, maximum actuator length

$\hat{n} = \hat{X}_P$ — Top platform normal

$\{n_x \quad n_y \quad n_z\}^T$ — Components of $\hat{n}$

$\tilde{n}_x$ — $1 + n_x$

N, N_1, N_2, N_3 — Cross longeron face normal length

$^B O_i : O_1, O_2, O_3$ — Stewart platform revolute locations

$O_{iy}, O_{iz}; i = 1,2,3$ — Components of O_1, O_2, O_3

p — Length from $\{B\}$ to $\{P\}$

p_0 — Difference of p and joint offset S

$^B q_i : q_1, q_2, q_3$ — Cross longeron face unit directions

$^B Q_i : Q_1, Q_2, Q_3$ — Lower actuation plane nodes

$\overline{Q_i Q_j}$ — Length from Q_i to Q_j

Q_{1R}, Q_{2R}, Q_{3R} — Upper actuation plane nodes

r — Gimbal extension parameter

S — VGT mid-plane joint offset

$\left[{}^B_P T \right]$ — Homogeneous transformation matrix, $\{P\}$ in $\{B\}$

$\hat{U}_1 = \{ U_{1x} \quad U_{1y} \quad U_{1z} \}^T$ — Mid-plane normal

$\hat{X}_B$ — Base normal

$\hat{X}_B, \hat{Y}_B, \hat{Z}_B$ — Unit vectors of $\{B\}$

$\hat{X}_P, \hat{Y}_P, \hat{Z}_P$ — Unit vectors of $\{P\}$

α, β — Gimbal angles

ϕ_1, ϕ_2, ϕ_3 — Angles of projections of q_1, q_2, q_3 onto base

$\theta_1, \theta_2, \theta_3$ — Cross longeron face angles

$(\theta_i)_{1,2}$ — Two inverse position solutions to θ_i

$\|x\|$ — Euclidean norm of vector x

3. DOUBLE OCTAHEDRAL VGT AS AN EXTENSIBLE GIMBAL

The NASA VGT module shown in Fig. 1 can be controlled as a two-axis gimbal (universal joint) with extension capability. Figure 2 shows the kinematic model for the VGT. As shown in Appendix A, the VGT has three degrees of freedom (DOF): there are three independently controlled linear actuators $L_1, L_2 L_3$. To provide three DOF, the design of joints connecting links at the VGT mid-plane is critical. Rhodes and Mikulas (1985) present the first VGT joint designs based on slotted spherical joints. Tidwell (1989) presents another design based on universal joints. Padmanabhan, et. al., (1992) present a good overview of VGT joint design. The NASA VGT hardware has mid-plane joints constructed with universal joints, but the details differ from Tidwell (1989). A promising alternative spherical joint design has recently been proposed by Hamlin and Sanderson (1994).

Since the VGT has three DOF, three output parameters can be controlled. There are five possible Cartesian output parameters to control (x, y, and z translations of a point on the platform with respect to the base, and pitch and yaw rotations about the Z_P and Y_P axes, respectively). The roll rotation about X_P is not possible with the VGT. For motion control, one possibility is to control the translation of a point on {P} with respect to the origin of {B}, as presented in Padmanabhan, et. al., (1990). With this scenario, the rotations cannot be controlled.

In this paper, the three output parameters are the pitch and yaw angles, plus the length of the joint. The VGT in Fig. 2 is modeled as the two-axis gimbal shown in Fig. 3. The variable length of the virtual gimbal joint, r, is the third freedom. This extension is not available in conventional gimbal designs which provide only the pitch and yaw angles. In addition, the stiffness and load-bearing characteristics of the VGT are superior to conventional gimbals due to the parallel truss nature of VGTs compared to the serial gearbox design of conventional gimbals. The intersection point of the two gimbal axes is fixed with respect to the VGT model. The lower and upper gimbal joint lengths (r in Fig. 3) are equal due to symmetry.

The three degree-of-freedom VGT can be used as a joint in a VGT-based manipulator. Such a manipulator could be controlled as a series of pitch-yaw joints with extension. The extension r can be constrained to be a constant, intermediate value for simpler manipulator kinematics. This case effectively maps the three degrees of freedom

6

to two output parameters (pitch and yaw). However, better performance may be possible if the extension r is also actively controlled.
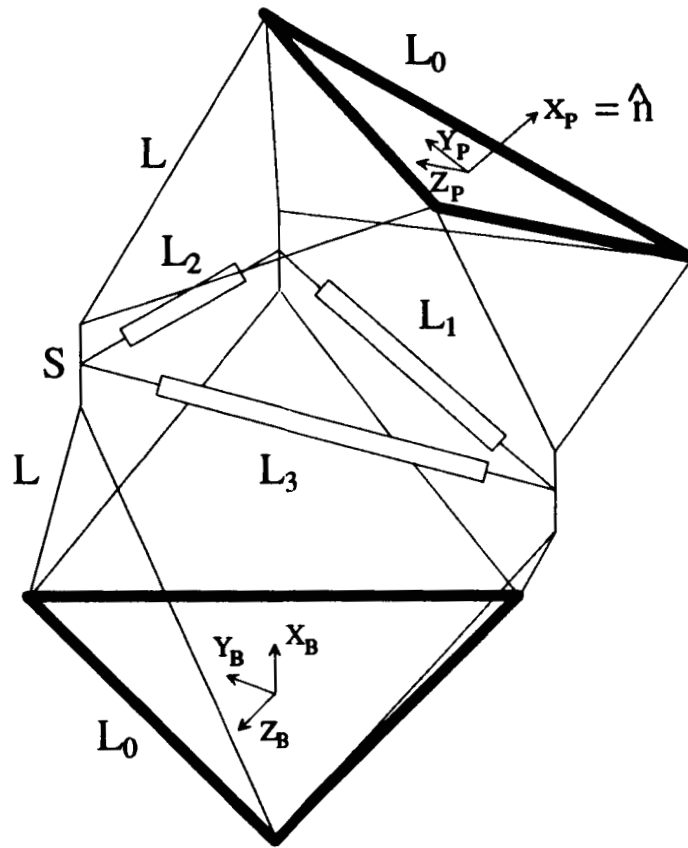

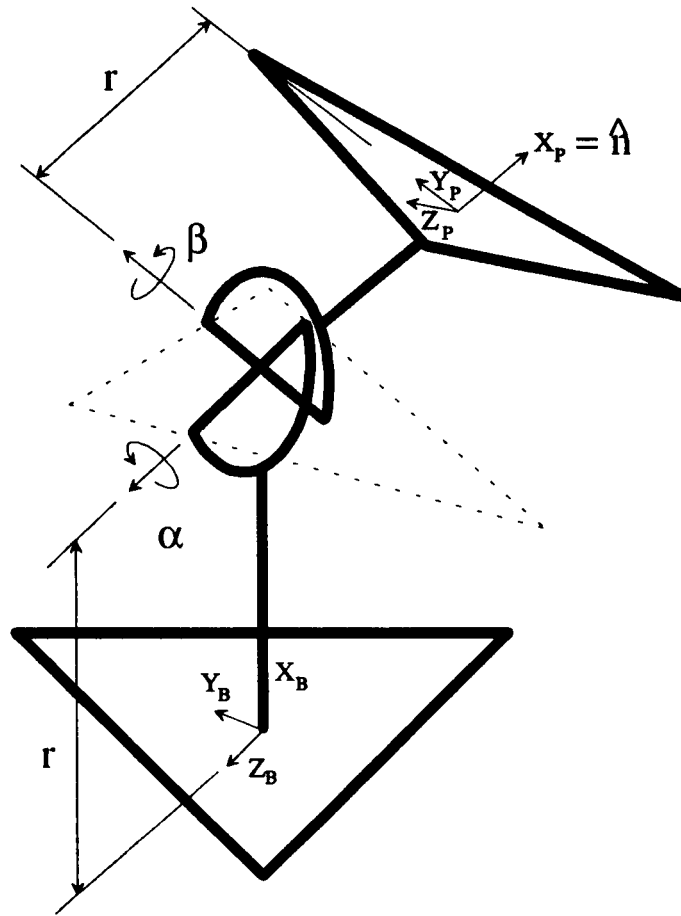*Figure 2*
Double Octahedral VGT Kinematic Diagram

Figure 3
Extensible Gimbal Kinematic Diagram

4. DOUBLE OCTAHEDRAL VGT POSITION KINEMATICS

This section formulates and solves the complete forward and inverse position equations for the VGT. The VGT input parameters are L_1, L_2, L_3 and the output parameters are α, β, r. The forward problem calculates α, β, r given L_1, L_2, L_3, while the inverse problem calculates L_1, L_2, L_3 given α, β, r, as illustrated in Fig. 4. The forward solution is useful for simulation and the inverse solution is used primarily for control. Both are used for VGT design and analysis.
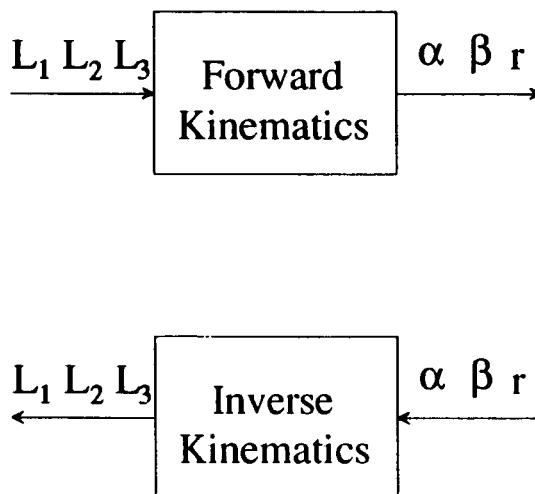
$$L_1\ L_2\ L_3 \longrightarrow \boxed{\begin{array}{c} \text{Forward} \\ \text{Kinematics} \end{array}} \xrightarrow{\ \alpha\ \beta\ r\ }$$

$$L_1\ L_2\ L_3 \longleftarrow \boxed{\begin{array}{c} \text{Inverse} \\ \text{Kinematics} \end{array}} \xleftarrow{\ \alpha\ \beta\ r\ }$$

Figure 4

Position Kinematics of the VGT as an Extensible Gimbal

Figure 5 shows intermediate details of Fig. 4. Each block in Fig. 5 is described in the following subsections. The VGT Forward A solution of Section 4.1.1 calculates the cross longeron face angles $\theta_1, \theta_2, \theta_3$ given the input parameters L_1, L_2, L_3. The VGT Forward B solution in Section 4.1.2 calculates the pointing vector $\hat{n}$ and the gimbal extension r given $\theta_1, \theta_2, \theta_3$. To finish the forward solution, the Gimbal Inverse solution in Section 4.3.2 calculates the gimbal angles α, β given $\hat{n}$; the gimbal extension r is unchanged. This solution is inverse because α, β are gimbal inputs while $\hat{n}$ is output. The VGT inverse solutions are accomplished using the same intermediate variables, in reverse order. The Gimbal Forward solution is presented in Section 4.3.1, VGT Inverse A in Section 4.2.1, and VGT Inverse B in Section 4.2.2.

Both the VGT forward and inverse solutions exploit the symmetry inherent in the design of Fig. 2. As explained in Padmanabhan, et. al., (1992), the actuator plane $L_1 - L_2 - L_3$ is a plane of symmetry. Due to the specific VGT geometry, the motion of the

9

top platform is a mirror image of the base, reflected about this plane of symmetry. Likewise each VGT longeron has a symmetric partner about this plane.
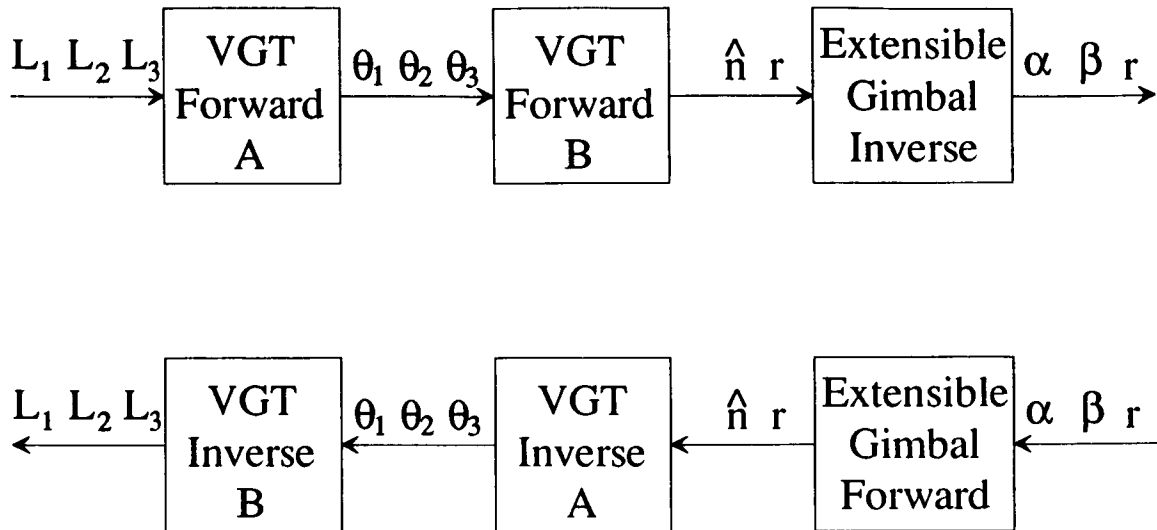

Figure 5

Position Kinematics of the VGT as an Extensible Gimbal:

Intermediate Variables

There are five length parameters for this VGT design (see Fig. 2): (1) Six bottom and top fixed battens L_0. The geometry is shown in Figs. B.1 and B.2; (2) Twelve fixed cross longerons L. The geometry for the cross longeron faces is shown in Figs. B.3 and B.4; (3) Minimum actuator extension L_{MIN}; (4) Maximum actuator extension L_{MAX}. The three actuators are identical; (5) Joint offset S separating pairs of cross longeron faces about the plane of symmetry. If a different parameter set was chosen for a VGT design, the desirable symmetry condition might not result.

4.1 VGT Forward Position Solution

This section presents the two VGT forward position solutions; given L_1, L_2, L_3, calculate $\hat{n}, r$. The gimbal inverse solution (Section 4.3.2) is then required to complete the VGT forward solution. As shown in Fig. 5, the VGT forward solution is divided into solutions A and B, separated by intermediate variables $\theta_1, \theta_2, \theta_3$.

4.1.1 VGT Forward A.

In this section, the solution for cross longeron face angles $\theta_1, \theta_2, \theta_3$ is obtained, given input parameters L_1, L_2, L_3. Only the half of the VGT under the plane of symmetry is solved. Then the position of the top half is determined by symmetry. This solution was presented by Padmanabhan, et. al., (1992), where three RSSR mechanisms (R-revolute joint; S-spherical joint) $O_1 Q_1 Q_2 O_2$, $O_2 Q_2 Q_3 O_3$, $O_3 Q_3 Q_1 O_1$

were identified and solved simultaneously (see Fig. 6b). An equivalent solution recognizes that the VGT configuration under the plane of symmetry is a Stewart's platform, with different actuation: the cross longerons are fixed and the platform lengths are actuated. The forward position solution for the Stewart platform is presented in Williams (1992). This solution is adapted for the VGT below.
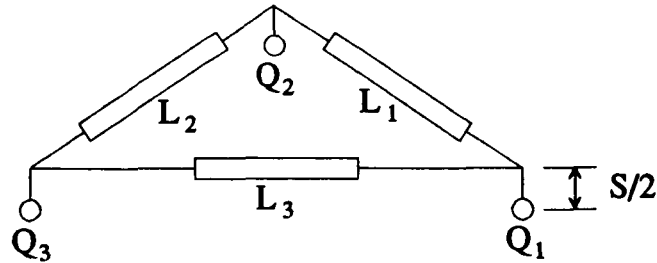

Figure 6a
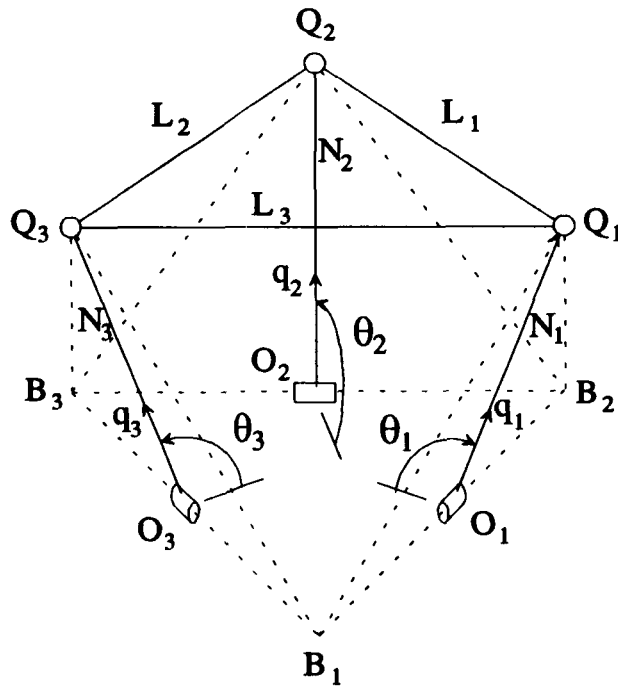
Stewart Platform Analogy: Offset Detail

Figure 6b

Stewart Platform Analogy

Figure 6b shows the Stewart platform analogy for the lower VGT half. The VGT joint offset S does not affect this solution because the plane connecting points Q_1, Q_2, Q_3 is parallel to the plane of symmetry. Therefore, virtual links L_1, L_2, L_3 connect points Q_1, Q_2, Q_3 to form the Stewart platform; see Figs. 6a and 6b. Figure 6b shows the definition of the cross longeron face angles $\theta_1, \theta_2, \theta_3$, measured from the base plane to the

virtual links O_iQ_i, about the base fixed batten directions. In Fig. 6b, the solid links are virtual, while the dotted links are actual VGT links. All links are fixed except for L_1, L_2, L_3, which are given.

Three scalar constraint equations are written, stating that L_1, L_2, L_3 are the lengths separating points Q_1, Q_2, Q_3:

$$L_1^2 = \overline{Q_1 Q_2} = \left\| {}^B Q_2 - {}^B Q_1 \right\|^2$$

$$L_2^2 = \overline{Q_2 Q_3} = \left\| {}^B Q_3 - {}^B Q_2 \right\|^2 \qquad (1)$$

$$L_3^2 = \overline{Q_3 Q_1} = \left\| {}^B Q_1 - {}^B Q_3 \right\|^2$$

where:

$$ {}^B Q_i = {}^B O_i + N_i \, {}^B q_i. \qquad (2)$$

The fixed locations ${}^B O_i$ and lengths N_i are given in Appendix B. The variable unit vector directions ${}^B q_i$ pointing along $O_i Q_i$ are functions of $\theta_1, \theta_2, \theta_3$, given in Eq. 3 ($s_i = \sin \theta_i$ and $c_i = \cos \theta_i$).

$$ {}^B q_i = \begin{Bmatrix} s_i \\ -c_i c\phi_i \\ -c_i s\phi_i \end{Bmatrix} \qquad (3)$$

From Fig. B.1, $\phi_1 = 180°, \phi_2 = 300°, \phi_3 = 60°$. Therefore,

$$ {}^B q_1 = \begin{Bmatrix} s_1 \\ c_1 \\ 0 \end{Bmatrix}, \quad {}^B q_2 = \begin{Bmatrix} s_2 \\ -\dfrac{1}{2} c_2 \\ \dfrac{\sqrt{3}}{2} c_2 \end{Bmatrix}, \quad {}^B q_3 = \begin{Bmatrix} s_3 \\ -\dfrac{1}{2} c_3 \\ -\dfrac{\sqrt{3}}{2} c_3 \end{Bmatrix} \qquad (4)$$

$$ {}^B Q_1 = \begin{Bmatrix} N s_1 \\ O_{1y} + N c_1 \\ 0 \end{Bmatrix}, \quad {}^B Q_2 = \begin{Bmatrix} N s_2 \\ O_{2y} - \dfrac{N}{2} c_2 \\ O_{2z} + \dfrac{\sqrt{3} N}{2} c_2 \end{Bmatrix}, \quad {}^B Q_3 = \begin{Bmatrix} N s_3 \\ O_{3y} - \dfrac{N}{2} c_3 \\ O_{3z} - \dfrac{\sqrt{3} N}{2} c_3 \end{Bmatrix}. \qquad (5)$$

12

Upon substitution, the three constraint equations become:

$$D_1 c_1 + D_2 c_2 + D_3 c_1 c_2 + D_4 s_1 s_2 + D_5 = 0$$
$$E_1 c_2 + E_2 c_3 + E_3 c_2 c_3 + E_4 s_2 s_3 + E_5 = 0 \qquad (6)$$
$$F_1 c_3 + F_2 c_1 + F_3 c_3 c_1 + F_4 s_3 s_1 + F_5 = 0$$

where:

$$D_1 = 2N\left(O_{1y} - O_{2y}\right)$$
$$D_2 = N\left(O_{1y} - O_{2y} + \sqrt{3}O_{2z}\right)$$
$$D_3 = N^2$$
$$D_4 = -2N^2 \qquad (6A$$
$$D_5 = \left(O_{1y} - O_{2y}\right)^2 + O_{2z}^2 + 2N^2 - L_1^2$$

$$E_1 = N\left(-\left(O_{2y} - O_{3y}\right) + \sqrt{3}\left(O_{2z} - O_{3z}\right)\right)$$
$$E_2 = N\left(\left(O_{2y} - O_{3y}\right) + \sqrt{3}\left(O_{2z} - O_{3z}\right)\right)$$
$$E_3 = N^2$$
$$E_4 = -2N^2 \qquad (6B$$
$$E_5 = \left(O_{2y} - O_{3y}\right)^2 + \left(O_{2z} - O_{3z}\right)^2 + 2N^2 - L_2^2$$

$$F_1 = N\left(O_{1y} - O_{3y} - \sqrt{3}O_{3z}\right)$$
$$F_2 = 2N\left(O_{1y} - O_{3y}\right)$$
$$F_3 = N^2$$
$$F_4 = -2N^2 \qquad (6c)$$
$$F_5 = \left(O_{1y} - O_{3y}\right)^2 + O_{3z}^2 + 2N^2 - L_3^2$$

The three constraint equations simplify to:

$$c_1 + c_2 + Ac_1 c_2 - 2As_1 s_2 + B = 0$$
$$c_2 + c_3 + Ac_2 c_3 - 2As_2 s_3 + C = 0 \qquad (7)$$
$$c_3 + c_1 + Ac_3 c_1 - 2As_3 s_1 + D = 0$$

where:

$$A = \frac{D_3}{D_1} = -\frac{2\sqrt{3}N}{3L_0}$$

$$B = \frac{D_5}{D_1} = \frac{A}{N^2}\left(E - L_1^2\right)$$

$$C = \frac{E_5}{D_1} = \frac{A}{N^2}\left(E - L_2^2\right)$$

$$D = \frac{F_5}{D_1} = \frac{A}{N^2}\left(E - L_3^2\right)$$

$$E = \frac{L_0^2}{4} + 2N^2$$

Equations 7 are three coupled non-linear equations in transcendentals of the unknowns $\theta_1, \theta_2, \theta_3$. Due to the symmetric VGT geometry, the coefficients of Eqs. 7 are simple compared to Eqs. 6. However, the basic structure of the solution is unchanged: there are 16 theoretical solutions (Nanua, et. al., 1990). Actually, there are 8 potentially useful solutions; the remaining 8 solutions are symmetric about the base plane.

For most simulation and control purposes, only one solution (closest to the previous configuration) is required. Therefore, in this paper, Eqs. 7 are solved numerically using the Newton-Raphson method. Appendix C presents adaptation of the Newton-Raphson method to solve for $\theta_1, \theta_2, \theta_3$.

4.1.2 VGT Forward B.
The pointing vector $\hat{n}$ and the gimbal extension r are calculated in this section given the cross longeron face angles $\theta_1, \theta_2, \theta_3$, where $\hat{n}$ is the normal to the VGT top platform, at its centroid. Symmetry is exploited to obtain the solution. This general solution was presented by Padmanabhan, et. al., (1992). Figure 7 gives the vector diagram for this solution.

Given $\theta_1, \theta_2, \theta_3$, $^B Q_i$ are calculated using Eq. 5. Then the unit vector directed from the origin of {B} to the origin of {P} can be found with Eq. 8. This unit vector $\hat{U}_1$ is normal to the actuation plane of symmetry. The total length from the base to the top platform along this vector is p.

$$\hat{U}_1 = \frac{\left(^B Q_2 - ^B Q_1\right) \times \left(^B Q_3 - ^B Q_1\right)}{\left\|\left(^B Q_2 - ^B Q_1\right) \times \left(^B Q_3 - ^B Q_1\right)\right\|} = \begin{Bmatrix} U_{1x} \\ U_{1y} \\ U_{1z} \end{Bmatrix} \tag{8}$$
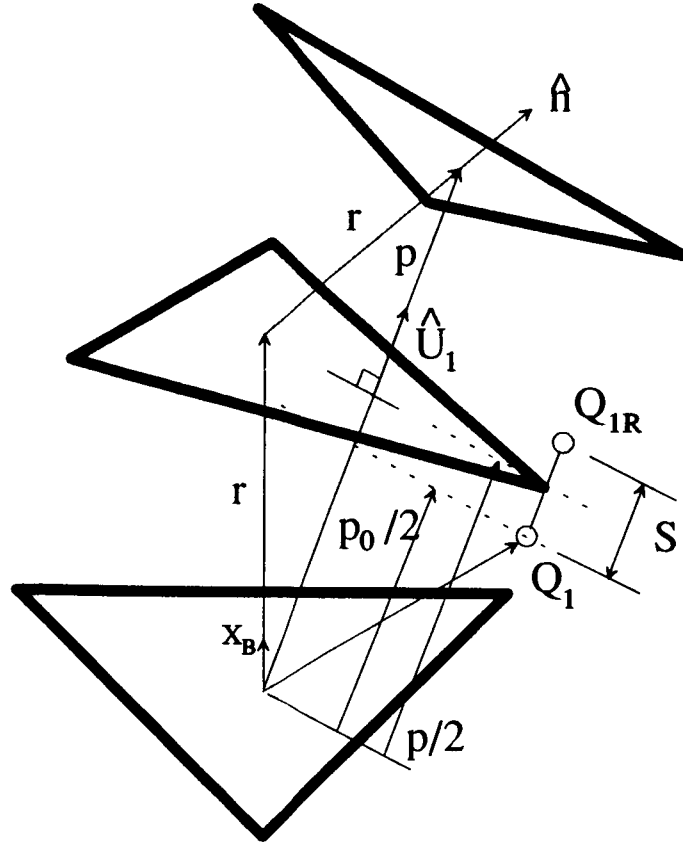
Figure 7
VGT Forward B Vector Diagram

The projection of r along $\hat{U}_1$ is $\dfrac{p}{2}$; this yields the following condition:

$$r = \frac{p}{2\hat{X}_B \cdot \hat{U}_1} \qquad (9)$$

where $\hat{X}_B = \{1 \quad 0 \quad 0\}^T$, thus:

$$r = \frac{p}{2U_{1x}}. \qquad (10)$$

To calculate r, we need p. The projection of $^B Q_1$ onto $\hat{U}_1$ is:

$$\frac{p_0}{2} = {}^B Q_1 \cdot \hat{U}_1. \qquad (11)$$

Since $\hat{U}_1$ is normal to the mid-plane, the joint offset S is parallel to it. Therefore, the distance to the mid-plane along $\hat{U}_1$ is:

$$\frac{p}{2} = \frac{p_0}{2} + \frac{S}{2}.$$ (12)

Substituting Eq. 11 into Eq. 12 and simplifying yields Eq. 13. Using this expression for p, r is determined from Eq. 10.

$$p = 2^B Q_1 \cdot \hat{U}_1 + S$$ (13)

To determine $\hat{n}$, the following vector loop closure equation is written.

$$r\hat{X}_B + r\hat{n} = p\hat{U}_1$$ (14)

Solving,

$$\hat{n} = \frac{p}{r}\hat{U}_1 - \hat{X}_B.$$ (15)

The expression for $\hat{n}$ in Eq. 15 is a unit vector, as proven below (making use of Eq. 10).

$$\hat{n} = \frac{p 2 U_{1x}}{p} \hat{U}_1 - \hat{X}_B = 2U_{1x}\hat{U}_1 - \hat{X}_B = \begin{Bmatrix} 2U_{1x}^2 - 1 \\ 2U_{1x}U_{1y} \\ 2U_{1x}U_{1z} \end{Bmatrix}$$ (16)

$$\|\hat{n}\| = \sqrt{4U_{1x}^2\left(U_{1x}^2 + U_{1y}^2 + U_{1z}^2 - 1\right) + 1} = \sqrt{4U_{1x}^2(0) + 1} = 1$$ (17)

For each of the sixteen possible $\theta_1, \theta_2, \theta_3$ solutions from Section 4.1.1, there is one $\hat{n}, r$ solution.

4.2 VGT Inverse Position Solution

This section presents the two VGT inverse position solutions; given $\hat{n}, r$, calculate L_1, L_2, L_3. First, however, the gimbal forward solution (Section 4.3.1) is required to start the VGT inverse solution. As shown in Fig. 5, the VGT inverse solution is divided into solutions A and B, separated by intermediate variables $\theta_1, \theta_2, \theta_3$.

4.2.1 VGT Inverse A. The cross longeron face angles $\theta_1, \theta_2, \theta_3$ are calculated in this section given the pointing vector $\hat{n}$ and the gimbal extension r. Symmetry is exploited to obtain the solution. Figure 8 gives the vector diagram for this solution. A similar solution was presented by Padmanabhan, et. al., (1992).
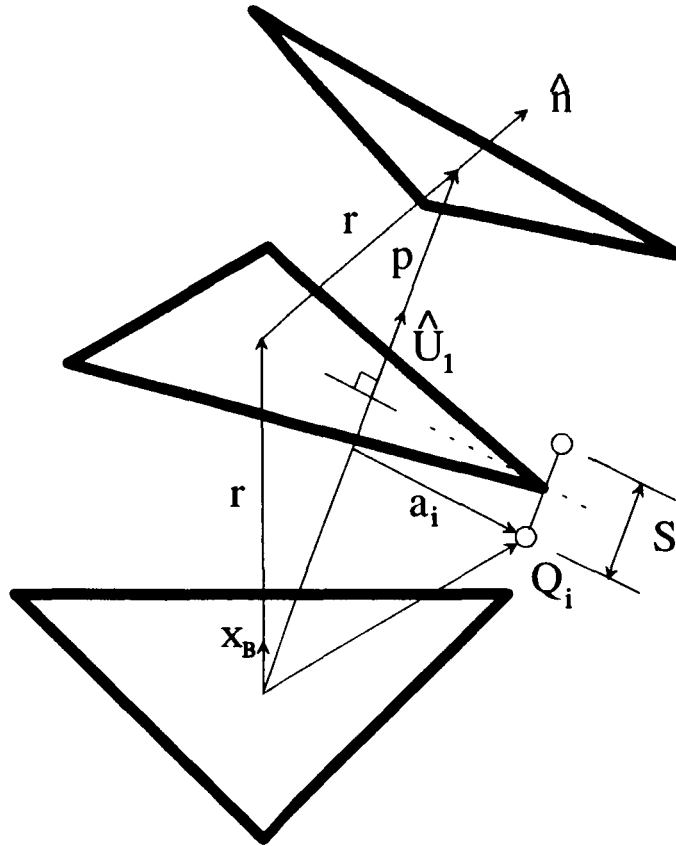

Figure 8
VGT Inverse A Vector Diagram

The unknown angles $\theta_1, \theta_2, \theta_3$ determine the vector locations $^B Q_i, i = 1, 2, 3$, respectively (see Fig. 6B. The following three scalar constraint equations are written (see Fig. 8):

$$a_i \cdot \hat{U}_1 = 0, i = 1, 2, 3 \tag{18}$$

Equations 18 state that each $^B Q_i, i = 1, 2, 3$ must lie on a plane parallel to the actuation plane. That is, a_i (the vector locating $^B Q_i$ in the plane offset by $\dfrac{S}{2}$ parallel to the actuation

plane) must be perpendicular to $\hat{U}_1$ (the normal to the actuation plane). From Figs. 7 and 8, the following vector equation is written:

$$^{B}Q_i = \frac{^{B}P}{2} - \frac{S}{2}\hat{U}_1 + a_i, i = 1,2,3 \tag{19}$$

where $^{B}P = p\hat{U}_1$. Equations 18 become:

$$\left(^{B}Q_i - \frac{^{B}P}{2} + \frac{S}{2}\hat{U}_1 \right) \cdot \hat{U}_1 = 0, i = 1,2,3. \tag{20}$$

The vectors $^{B}Q_i, i = 1,2,3$ are given symbolically in Eq. 5. Equation 14 is rewritten to yield ^{B}P:

$$^{B}P = r\left(\hat{X}_B + \hat{n} \right). \tag{21}$$

With r, $\hat{X}_B = \{1 \quad 0 \quad 0\}^T$, and $\hat{n} = \{n_x \quad n_y \quad n_z\}^T$ given, ^{B}P is known:

$$^{B}P = r\left\{ \begin{matrix} 1+n_x \\ n_y \\ n_z \end{matrix} \right\}. \tag{22}$$

Now the actuation plane normal can be calculated:

$$\hat{U}_1 = \frac{^{B}P}{\left\| ^{B}P \right\|}. \tag{23}$$

where:

$$\left\| ^{B}P \right\| = r\sqrt{1 + 2n_x + n_x^2 + n_y^2 + n_z^2} = r\sqrt{2(1+n_x)} \tag{24}$$

Substituting Eq. 23 into Eq. 20 yields the following three constraint equations.

$$\left(^{B}Q_i - \frac{^{B}P}{2} \right) {}^{B}P + \frac{S}{2} \left\| ^{B}P \right\| = 0, i = 1,2,3 \tag{25}$$

18

Substituting Eqs. 5, 22, and 24, into Eqs. 25, the three constraint equations become:

$$E_1 c_1 + F_1 s_1 + G_1 = 0$$
$$E_2 c_2 + F_2 s_2 + G_2 = 0 \qquad (26)$$
$$E_3 c_3 + F_3 s_3 + G_3 = 0$$

where:

$$E_1 = Nrn_y$$

$$F_1 = Nr(1 + n_x) \qquad (26a)$$

$$G_1 = r\left(n_y O_{1y} - r(1 + n_x) + S\sqrt{\frac{1 + n_x}{2}} \right)$$

$$E_2 = -Nr\left(\frac{1}{2} n_y - \frac{\sqrt{3}}{2} n_z \right)$$

$$F_2 = Nr(1 + n_x) \qquad (26b)$$

$$G_2 = r\left(n_y O_{2y} + n_z O_{2z} - r(1 + n_x) + S\sqrt{\frac{1 + n_x}{2}} \right)$$

$$E_3 = -Nr\left(\frac{1}{2} n_y + \frac{\sqrt{3}}{2} n_z \right)$$

$$F_3 = Nr(1 + n_x) \qquad (26c)$$

$$G_3 = r\left(n_y O_{3y} + n_z O_{3z} - r(1 + n_x) + S\sqrt{\frac{1 + n_x}{2}} \right)$$

Defining $\tilde{n}_x = 1 + n_x$, and dividing by r, the three constraint equations simplify to:

$$E_1 c_1 + F_1 s_1 + G_1 = 0$$
$$E_2 c_2 + F_1 s_2 + G_2 = 0 \qquad (27)$$
$$E_3 c_3 + F_1 s_3 + G_3 = 0$$

$$E_1 = Nn_y$$

$$F_1 = N\tilde{n}_x \tag{27a}$$

$$G_1 = -r\tilde{n}_x - \frac{L_0}{2\sqrt{3}}n_y + S\sqrt{\frac{\tilde{n}_x}{2}}$$

$$E_2 = -\frac{N}{2}\left(n_y - \sqrt{3}n_z\right)$$

$$G_2 = -r\tilde{n}_x + \frac{L_0}{4}\left(\frac{1}{\sqrt{3}}n_y - n_z\right) + S\sqrt{\frac{\tilde{n}_x}{2}} \tag{27b}$$

$$E_3 = -\frac{N}{2}\left(n_y + \sqrt{3}n_z\right)$$

$$G_3 = -r\tilde{n}_x + \frac{L_0}{4}\left(\frac{1}{\sqrt{3}}n_y + n_z\right) + S\sqrt{\frac{\tilde{n}_x}{2}} \tag{27c}$$

Using the tangent half-angle substitution ($t = \tan\frac{\theta_i}{2}$, $\cos\theta_i = \frac{1-t^2}{1+t^2}$, $\sin\theta_i = \frac{2t}{1+t^2}$), the general solution to $E_i\cos\theta_i + F_i\sin\theta_i + G_i = 0$ is given in Eq. 28.

$$\left(\theta_i\right)_{1,2} = 2\tan^{-1}\left(\frac{-F_i \pm \sqrt{E_i^2 + F_i^2 - G_i^2}}{G_i - E_i}\right) \tag{28}$$

Due to the multiplicative factor 2 in Eq. 28, the quadrant-specific atan2 function need not be used. However, due to the quadratic degree of the tangent half-angle substitution, there are two possible solutions for each θ_i (the $\pm$ in Eq. 28). Since each θ_i is solved independently of the other two, there are a total of eight (2^3) possible solutions to the VGT Inverse A problem. This means that in general, eight distinct VGT configurations exist to yield the same $\hat{n}, r$. For the physical VGT hardware modeled in the examples (Section 5), extensive computer simulation reveals there is only one valid inverse solution when joint limits are considered. This solution corresponds to choosing $\left(\theta_i\right)_2, i = 1,2,3$.

4.2.2 VGT Inverse B.

The leg lengths L_1, L_2, L_3 are calculated in this section given the cross longeron face angles $\theta_1, \theta_2, \theta_3$. First, given $\theta_1, \theta_2, \theta_3$, the vector locations $^B Q_i, i = 1,2,3$ are calculated from Eq. 5. Then the Euclidean norm is used to calculate L_i.

$$L_1 = \left\| {}^{B}Q_2 - {}^{B}Q_1 \right\|$$

$$L_2 = \left\| {}^{B}Q_3 - {}^{B}Q_2 \right\| \tag{29}$$

$$L_3 = \left\| {}^{B}Q_1 - {}^{B}Q_3 \right\|$$

Given each $\theta_1, \theta_2, \theta_3$ from the VGT Inverse A solution, there is a unique L_1, L_2, L_3 because only the positive square root is allowed.

4.3 Extensible Gimbal Position Kinematics

In order to control the VGT as a gimbal with extension, the kinematic equations of this virtual device are developed. Section 4.3.1 presents the gimbal forward solution, which is required to start the VGT inverse position solution (see Fig. 5). Section 4.3.2 presents the gimbal inverse solution, which is required to complete the VGT forward position solution. Figure 3 shows the kinematic model for the virtual extensible gimbal. The extensible gimbal position solutions relate the input parameters α, β, r to the output parameters $\hat{n}, r$ (the r transformation is identity). The normal to the top platform is $\hat{n}$ while the gimbal extension is r. The gimbal angles are α, β. The center of the virtual gimbal moves with respect to the VGT base. Section 4.3.3 presents the gimbal forward transform. Instead of $\hat{n}, r$, the output parameters here are $\left[{}^{B}_{P}T \right]$, the full homogeneous transformation matrix (Craig, 1989) relating $\{P\}$ in terms of $\{B\}$.

4.3.1 Extensible Gimbal Forward.
In this section, $\hat{n}, r$ are calculated given α, β, r. Appendix D gives the detailed extensible gimbal kinematic diagram and the associated Denavit-Hartenberg parameters. Using these Denavit-Hartenberg parameters in the forward kinematics, $\hat{n}$ is given in Eq. 30. $\left\{ {}^{B}\hat{X}_P \right\}$ is the unit direction $\hat{X}_P$ expressed in $\{B\}$:

$$\hat{n} = \left\{ {}^{B}\hat{X}_P \right\} = \begin{Bmatrix} c\alpha c\beta \\ s\alpha c\beta \\ -s\beta \end{Bmatrix} \tag{30}$$

The r transformation is identity. That is, r is viewed here as both an input and output parameter for the extensible gimbal. The following equation calculates the value of p,

which is the length from the origin of *{B}* to the origin of *{P}* (see Figs. 7 or 8). Equation 31 was derived from Eq. 24.

$$p = r\sqrt{2(1 + c\alpha c\beta)}$$ (31)

4.3.2 Gimbal Inverse. In this section, α, β, r are calculated given $\hat{n}, r$. Again, the r transformation is identity. To solve for α, β, the given $\hat{n} = \{n_x \quad n_y \quad n_z\}^T$ is equated to the expressions of Eq. 30. A ratio of the y and x terms yields α; $c\beta$ divides out, but its sign is unknown. Therefore, there are two possible α solutions:

$$\alpha_1 = A\tan 2\left(\frac{n_y}{n_x}\right)$$ (32A

$$\alpha_2 = A\tan 2\left(\frac{-n_y}{-n_x}\right) = \alpha_1 + \pi$$ (32B

A ratio of the z and x terms yields β; each α result yields a unique β, so there are two possible β solutions:

$$\beta_1 = A\tan 2\left(\frac{n_z c\alpha}{-n_x}\right)$$ (33A

$$\beta_2 = \beta_1 + \pi$$ (33B

The primary solution α_1, β_1 is in the range of interest for the VGT. With α_2, β_2, the origin of *{P}* and direction of $\hat{X}_P$ is the same (i.e. α_2, β_2 is a valid solution), but $\hat{Y}_P$ and $\hat{Z}_P$ are reversed.

4.3.3 Gimbal Forward Transform. In this section $\left[^B_P T\right]$ is calculated given α, β, r. $\left[^B_P T\right]$ is the homogeneous transformation matrix (Craig, 1989) giving the position and orientation of *{P}* relative to *{B}*. Since the virtual extensible gimbal has only three degrees of freedom, $\left[^B_P T\right]$ is a subspace of six-dimensional Cartesian space. The output parameters $\hat{n}, r$ are one possible output set to represent the three VGT degrees of freedom. $\left[^B_P T\right]$ gives the full Cartesian information for the VGT. This transformation

matrix is useful for VGT simulation and control. It is also required to calculate the VGT node locations (see Appendix E). Given the Denavit-Hartenberg parameters in Appendix D, $\left[{}^B_P T\right]$ is presented in Eq. 34. Note that the first column contains $\hat{n} = \left\{{}^B\hat{X}_P\right\}$.

$$\left[{}^B_P T\right] = \begin{bmatrix} c\alpha c\beta & -s\alpha & c\alpha s\beta & r(1+c\alpha c\beta) \\ s\alpha c\beta & c\alpha & s\alpha s\beta & rs\alpha c\beta \\ -s\beta & 0 & c\beta & -rs\beta \\ 0 & 0 & 0 & 1 \end{bmatrix} \tag{34}$$

4.4 VGT Node Locations

Following either VGT Forward or Inverse kinematic position solution, the VGT node locations can be calculated. These node locations are required for finite element analysis, VGT graphical simulation, and other types of analyses. The node location calculations are detailed in Appendix E.

23

5. EXAMPLES

Three examples are presented in this section to demonstrate the calculation of complete forward and inverse position kinematics for the VGT as an extensible gimbal. The three examples in this section are for the NASA VGT hardware, shown in Fig. 1. The five nominal parameters for this VGT are (inches):

$$L_0 = 36$$
$$L = 34$$
$$L_{MIN} = 36$$
$$L_{MAX} = 55.5$$
$$S = 4.75$$

These examples have been verified by computer simulation (inverse kinematics checking forward and vice versa) and with hardware measurements. Units for lengths are inches, units for angles are degrees, and $\hat{n}$ and the rotation matrix part of $\left[{}_P^B T \right]$ are dimensionless.

5.1 Example 1

When all input leg lengths are equal, the top platform remains horizontal. All variables in Fig. 5 are given below. These numbers may be reproduced with either forward or inverse kinematics.

$$L_1 = L_2 = L_3 = 45$$

$$\theta_1 = \theta_2 = \theta_3 = 122.7$$

$$\hat{n} = \{1 \quad 0 \quad 0\}^T$$

$$\alpha = \beta = 0 \qquad r = 26.64$$

5.2 Example 2

When two input leg lengths are minimum, and the other is maximum, a maximum gimbal angle case results. The possible combinations of L_{MIN}, L_{MAX} for all three input legs lengths yield the extreme gimbal angles (some are in combinations of α, β). The example below gives the maximum positive α for this VGT.

$$L_1 = L_3 = 36 \qquad L_2 = 55.5$$

$$\theta_1 = 79.1 \qquad \theta_2 = \theta_3 = 138.6$$

$$\hat{n} = \{.673 \quad .739 \quad 0\}^T$$

$$\alpha = 47.7 \qquad \beta = 0 \quad r = 28.73$$

5.3 Example 3

This is a general example within the motion range of the NASA VGT. For this case, $\left[{}^B_P T \right]$ is calculated. Also, Tables 1 and 2 present the multiple solutions of the VGT inverse problem. Each L_1, L_2, L_3 set in Table 2 was given as input to the forward kinematics, resulting in the same α, β, r for each solution. As seen in Table 2, only the last solution is valid when actuator joint limits $36 \le L_i \le 55.5$ are considered. This condition has been observed in all of the computer simulations which have been performed, which indicates that multiple solutions do not present a problem for control of the VGT as an extensible gimbal.

$$L_1 = 45 \qquad L_2 = 53 \qquad L_3 = 50$$

$$\theta_1 = 117.9 \qquad \theta_2 = 127.4 \qquad \theta_3 = 141.4$$

$$\hat{n} = \{.955 \quad .242 \quad .171\}^T$$

$$\alpha = 14.2 \qquad \beta = -9.8 \qquad r = 24.92$$

$$\left[{}^B_P T \right] = \begin{bmatrix} .955 & -.246 & -.166 & 48.73 \\ .242 & .969 & -.042 & 6.04 \\ .171 & 0 & .985 & 4.26 \\ 0 & 0 & 0 & 1 \end{bmatrix}$$

Table 1 Multiple θ_i Solutions

	θ_1	θ_2	θ_3
1	47.9	51.0	54.2
2	117.9	127.4	141.4

Table 2 Multiple L_i Solutions

	L_1	L_2	L_3
1	14.5	12.4	13.5
2	14.5	30.2	29.7
3	24.7	25.3	13.5
4	24.7	53.0	29.7
5	21.3	12.4	21.5
6	21.3	30.2	50.0
7	45.0	25.3	21.5
8	45.0	53.0	50.0

6. CONCLUSION

This paper presents the complete forward and inverse kinematic solutions for control of a three DOF double octahedral VGT module as an extensible gimbal. The results can be used for design, analysis, simulation, and control. A VGT can be used as a joint in a large, lightweight, high load-bearing VGT-based manipulator for earth- and space-based remote operations, plus industrial applications.

Using the Stewart platform analogy, there are eight possible solutions to the VGT forward position problem. However, in this paper, a numerical method is used for solution, which yields one solution, closest to the previous configuration. There are eight solutions to the VGT inverse position problem. All eight solutions are calculated in this paper, but it was observed that only one solution is valid when practical joint limits are considered.

The results of this work have been used to control the NASA VGT hardware as an extensible gimbal, to demonstrate the capability for this device as a joint in a VGT-based manipulator. This work is an integral part of a comprehensive VGT-based manipulator design, simulation, and control tool.

7. REFERENCES

Craig, J.J., 1989, **Introduction to Robotics: Mechanics and Control**, Second Edition, Addison-Wesley Publishing Company, Reading, MA.

Dahlquist, G., and Bjorck, A., 1974, **Numerical Methods**, Prentice-Hall, Inc., Englewood, NJ.

Hamlin, G.J. and Sanderson, A.C., 1994, *"A Novel Concentric Multilink Spherical Joint with Parallel Robotics Applications"*, proceedings of the **1994 IEEE Conference on Automation and Robotics**, Vol. 2, San Diego, CA, pp. 1267-1272.

Mabie, H.H., and Reinholtz, C.F., 1987, **Mechanisms and Dynamics of Machinery**, John Wiley & Sons, Inc., New York, Section 12.2.

Millsap, W.J., Salerno, R.J., Robertshaw, H.H., Horner, C.G., and Bennett, D.W., 1992, *"Proposed Use of a Variable Geometry Truss Manipulator for Radioactive Waste Removal from Underground Storage Tanks"*, **Proceedings of the Symposium on Waste Management**, Vol. 1, Tucson, AZ, pp. 849-853.

Nanua, P., Waldron, K.J., and Murthy, V., 1990, *"Direct Kinematic Solution of a Stewart Platform"*, **IEEE Transactions on Robotics and Automation**, Vol. 6, No. 4, pp. 438-443.

Padmanabhan, B., 1992, *"A Study of Isostatic Framework with Application to Manipulator Design"*, PhD Dissertation, Virginia Polytechnic Institute & State University, Blacksburg, VA.

Padmanabhan, B., Tidwell, P.H., Salerno, R.J., and Reinholtz, C.F., 1992, *"VGT-Based Gimbals: Practical Construction and General Theory"*, **Proceedings of the 1992 ASME Mechanisms Conference**, DE-Vol 47, Phoenix, AZ, pp. 437-443.

Padmanabhan, B., Arun, V., and Reinholtz, C.F., 1990, *"Closed-Form Inverse Kinematic Analysis of Variable Geometry Truss Manipulators"*, **Proceedings of the 1990 ASME Mechanisms Conference**, DE-Vol 26, Chicago, IL, pp. 99-105.

Rhodes, M.D., and Mikulas, M.M., Jr., 1985, *"Deployable Controllable Geometry Truss Beam"*, **NASA Technical Memorandum 86366**.

Tidwell, P.H., 1989, *"Design and Construction of a Double-Octahedral Variable-Geometry-Truss Manipulator"*, M.S. Thesis, Virginia Polytechnic Institute & State University, Blacksburg, VA.

Williams, R. L., II, 1992, *"Kinematics of an In-Parallel Actuated Manipulator Based on the Stewart Platform Mechanism"*, NASA Technical Memorandum 107585, NASA Langley Research Center, Hampton, VA.

Wynn, R.H., and Robertshaw, H.H., 1991, *"The Control of Flexible Structure Vibrations Using a Cantilevered Adaptive Truss"*, Proceedings of the AIAA / ASME / ASCE / ASC 32nd Structures, Structural Dynamics, and Materials Conference, AIAA Paper 91-1063-CP, pp. 2190-2196, Baltimore, MD.

APPENDIX A. VGT Mobility

The Kutzbach equation (Mabie and Reinholtz, 1987) is useful for calculating the spatial mobility (M) for a given device:

$$M = 6(N-1) - 5J_1 - 4J_2 - 3J_3 - 2J_4 - J_5 \qquad \text{(A.1)}$$

where M is the mobility, or number of degrees of freedom of a device, N is the number of links including the fixed link, and J_i is the number of i-DOF joints.

For a theoretical double octahedral VGT, all joints are modeled as spherical joints, and any strut may be linearly actuated. For the case of three actuators on the mid-plane, the mobility is:

$$M = 6(20-1) - 5(3) - 3(27) = 18. \qquad \text{(A.2)}$$

There are twenty links (top and bottom plates, twelve cross longerons, and two for each actuated link), three prismatic joints, and twenty-seven spherical joints (for each mid-plane node, six links theoretically join at one point; so five spherical joints are required). However, each link with spherical joints on each end has an idle DOF, rotation about its own axis. There are fifteen idle freedoms (twelve cross longerons and three actuators), so the effective mobility is $M = 18 - 15 = 3$.

For the specific NASA VGT hardware, the design goal was to replace as many spherical joints as possible while maintaining three DOF. To enumerate links and joints, consider a VGT subchain: one pair of cross longeron faces connecting the base plate to the top plate; e.g. connecting $B_3 B_1$ to $B_{3R} B_{1R}$ through Q_3 and Q_{3R} (see Fig. A.1). As shown in Fig. 6b, two cross longerons forming a face may be replaced with a kinematically equivalent single link, rotating about the base (or top) plate with a single revolute joint. The two cross longeron faces are connected by two universal joints, separated by the yoke. An idler rotates relative to the yoke. The two actuated links connect to the idler via two revolute joints. Therefore for each such subchain, there are six links, two universal joints (which are two-DOF joints), and five revolute joints. For the entire VGT, there are twenty links (six links per subchain times three subchains, plus the top and bottom plates), six universal joints, and eighteen one-DOF joints (five revolute joints per subchain times three subchains, plus three actuated prismatic joints). Therefore:

$$M = 6(20-1) - 5(18) - 4(6) = 0 \qquad \text{(A.3)}$$

This result predicts that the NASA VGT is a statically determinate truss with no freedom to move! The Kutzbach equation is known to fail when the device contains special planar geometry within its spatial arrangement. The VGT actuation mid-plane is a triangle. The actuator links connect to the idlers, which are always perpendicular to the actuation triangle. The Kutzbach equation does not know of this special arrangement and correctly predicts zero DOF (if these three idler axes were skew to each other, no motion would be possible). To get the correct results in the Kutzbach equation, the one-DOF prismatic actuators must be modeled as two-DOF cylindrical joints. This removes three joints from J_1 and adds them to J_2:

$$M = 6(20-1) - 5(15) - 4(9) = 3 \qquad \text{(A.4)}$$
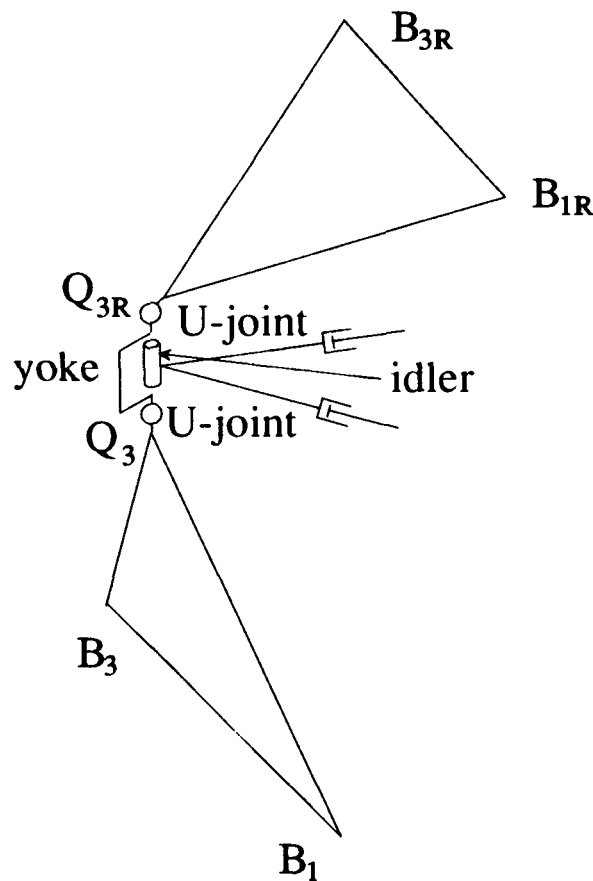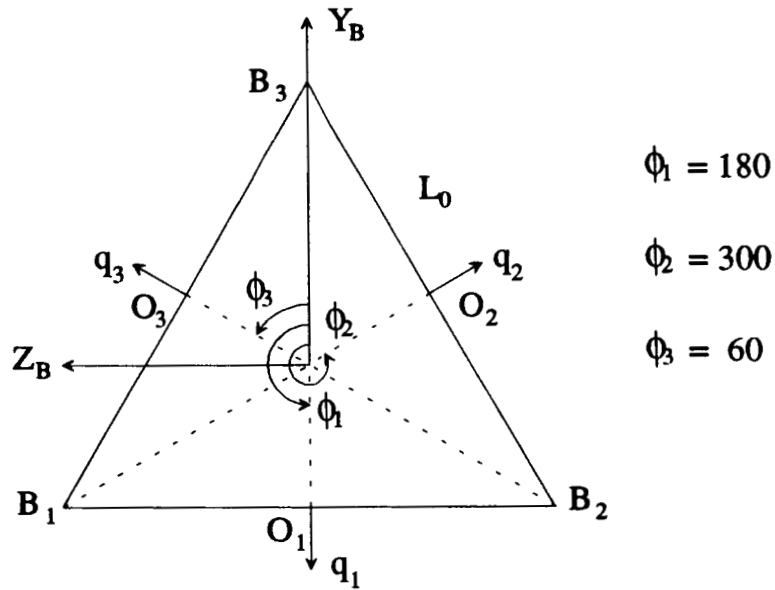
Thus the NASA VGT has three DOF.

Figure A.1 VGT Subchain

Fixed VGT Geometry

This appendix presents fixed VGT geometry for use in forward and inverse position analyses. Referring to Fig. 6b, the points ${}^B O_i = \{0 \quad O_{iy} \quad O_{iz}\}^T$ are the virtual revolute joint locations in the Stewart platform analogy. Fig. B.1 shows the details necessary to calculate these locations.

$$
{}^B O_1 = \left\{ \begin{array}{c} 0 \\ -\dfrac{L_0}{2\sqrt{3}} \\ 0 \end{array} \right\}
\qquad
{}^B O_2 = \left\{ \begin{array}{c} 0 \\ \dfrac{L_0}{4\sqrt{3}} \\ -\dfrac{L_0}{4} \end{array} \right\}
\qquad
{}^B O_3 = \left\{ \begin{array}{c} 0 \\ \dfrac{L_0}{4\sqrt{3}} \\ \dfrac{L_0}{4} \end{array} \right\}
\qquad (B.1)
$$

$\phi_1 = 180$

$\phi_2 = 300$

$\phi_3 = 60$

Figure B.1

VGT Base Geometry

As shown in Fig. B.2, the top platform geometry is identical to the base.
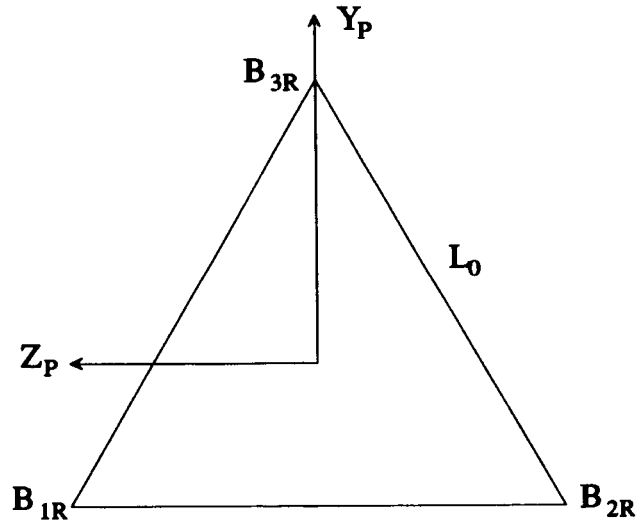
Figure B.2
VGT Top Platform Geometry

Figure B.3 shows one of the cross longeron planes. These three planes are identical, so:

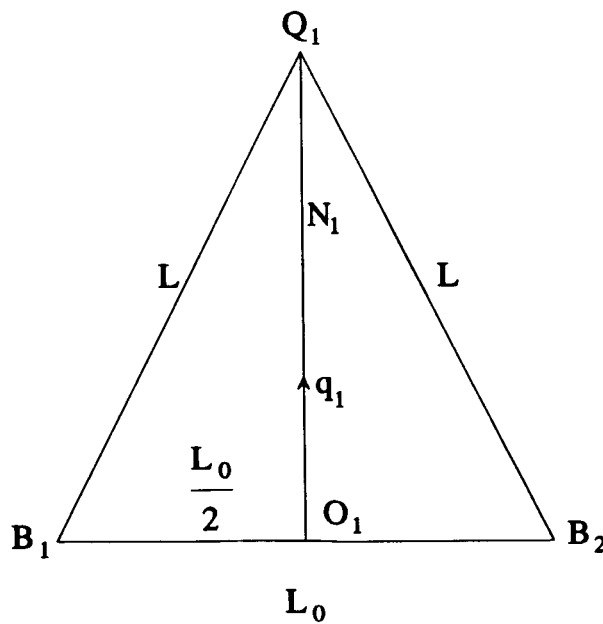$$N_1 = N_2 = N_3 = N = \sqrt{L^2 - \frac{L_0^2}{4}}.$$
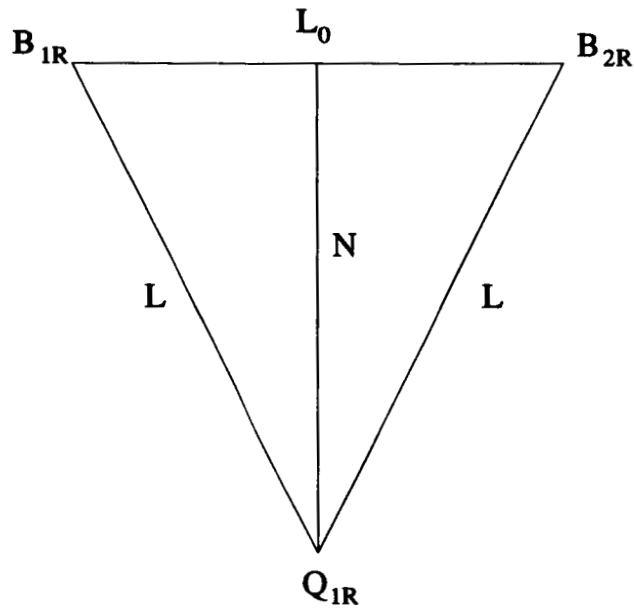
(B.2)

Figure B.3
Lower Cross Longeron Face Geometry

Figure B.4 shows that the upper cross longeron planes are symmetric to the lower.

Figure B.4
Upper Cross Longeron Face Geometry

Newton-Raphson Method
Applied to VGT Forward A Solution

This appendix presents numerical solution of Eqs. 7 using the Newton-Raphson method. These equations, arising in the VGT Forward A position analysis, are coupled and non-linear (transcendental). The general Newton-Raphson method for numerically solving non-linear systems of equations is discussed in Dahlquist and Bjorck (1974, Section 6.9.2). The Newton-Raphson method is applied by Williams (1992, Appendix C) to solve the forward position problem of the Stewart platform. In this appendix, the Newton-Raphson method is adapted to solve the VGT Forward A problem. It requires an initial guess which is "sufficiently close"; quadratic convergence is guaranteed under this condition. In real-time control, an excellent initial guess is the previous known configuration of the VGT. The VGT has eight possible forward kinematic solutions, but the method in this appendix only tracks one, closest to the previous configuration. The inverse Jacobian matrix is presented symbolically, so Gaussian elimination is not required.

Equations 7 are three coupled equations in transcendentals of the unknown cross longeron face angles $\Theta = \{\theta_1 \quad \theta_2 \quad \theta_3\}^T$, rewritten in Eqs. C.1 and C.2.

$$F_i(\Theta) = 0; i = 1, 2, 3 \tag{C.1}$$

$$
\begin{aligned}
F_1(\Theta) &= c_1 + c_2 + Ac_1c_2 - 2As_1s_2 + B = 0 \\
F_2(\Theta) &= c_2 + c_3 + Ac_2c_3 - 2As_2s_3 + C = 0 \\
F_3(\Theta) &= c_3 + c_1 + Ac_3c_1 - 2As_3s_1 + D = 0
\end{aligned}
\tag{C.2}
$$

The general Newton-Raphson iteration for step $k+1$ is summarized below.

$$J\delta\Theta_k = -F_i(\Theta_k) \tag{C.3}$$

The Jacobian matrix is a multi-dimensional form of the derivative:

$$J = \frac{\partial F_i}{\partial \theta_j} \tag{C.4}$$

Equation C.3 is solved for $\delta\Theta_k$, then the updated vector of unknowns is calculated with Eq. C.5.

$$\Theta_{k+1} = \Theta_k + \delta\Theta_k \qquad\qquad\qquad (C.5)$$

Iteration continues until $\|\delta\Theta_k\| < \varepsilon$, a user-defined tolerance. The method requires an initial guess, Θ_0, "sufficiently close" for convergence.

For the VGT, the Newton-Raphson Jacobian matrix is given below.

$$J = \begin{bmatrix} K_1 & K_3 & 0 \\ 0 & K_4 & K_6 \\ K_2 & 0 & K_5 \end{bmatrix} \qquad\qquad\qquad (C.6)$$

where:

$$K_1 = K_B s_1 + K_E c_1$$

$$K_2 = K_C s_1 + K_F c_1$$

$$K_3 = K_A s_2 + K_D c_2$$

$$K_4 = K_C s_2 + K_F c_2$$

$$K_5 = K_A s_3 + K_D c_3$$

$$K_6 = K_B s_3 + K_E c_3$$

$$K_A = -(1 + A c_1)$$

$$K_B = -(1 + A c_2)$$

$$K_C = -(1 + A c_3)$$

$$K_D = -2 A s_1$$

$$K_E = -2 A s_2$$

$$K_F = -2 A s_3$$

This Jacobian matrix is inverted symbolically, so Eq. C.3 is solved analytically as follows:

$$\delta\Theta_k = -J^{-1} F_i(\Theta_k) \qquad\qquad\qquad (C.7)$$

where:

$$J^{-1} = \frac{1}{DET} \begin{bmatrix} K_4 K_5 & -K_3 K_5 & K_3 K_6 \\ K_2 K_6 & K_1 K_5 & -K_1 K_6 \\ -K_2 K_4 & K_2 K_3 & K_1 K_4 \end{bmatrix} \qquad\qquad\qquad (C.8)$$

$$DET = K_1 K_4 K_5 + K_2 K_3 K_6 \qquad\qquad\qquad (C.9)$$

APPENDIX D. Virtual Extensible Gimbal Kinematic Details

This appendix presents the Denavit-Hartenberg parameters and the associated kinematic figure for the virtual extensible gimbal. This information was used to derive $\left\{{}^{B}\hat{X}_P\right\}$ for Sections 4.3.1 and 4.3.2, and $\left[{}^{B}_{P}T\right]$ in Section 4.3.3 and Appendix E. For the coordinate frame assignments shown in Fig. D.1, Table D.1 gives the Denavit-Hartenberg parameters (Craig, 1989, convention) for the extensible gimbal. The gimbal angles are α, β and r is the symmetric gimbal extension.

Table D.1 Extensible Gimbal D-H Parameters

i	α_{i-1}	a_{i-1}	d_i	θ_i
1	0	r	0	0
2	0	0	0	α
3	$-90°$	0	0	β
4	$90°$	r	0	0
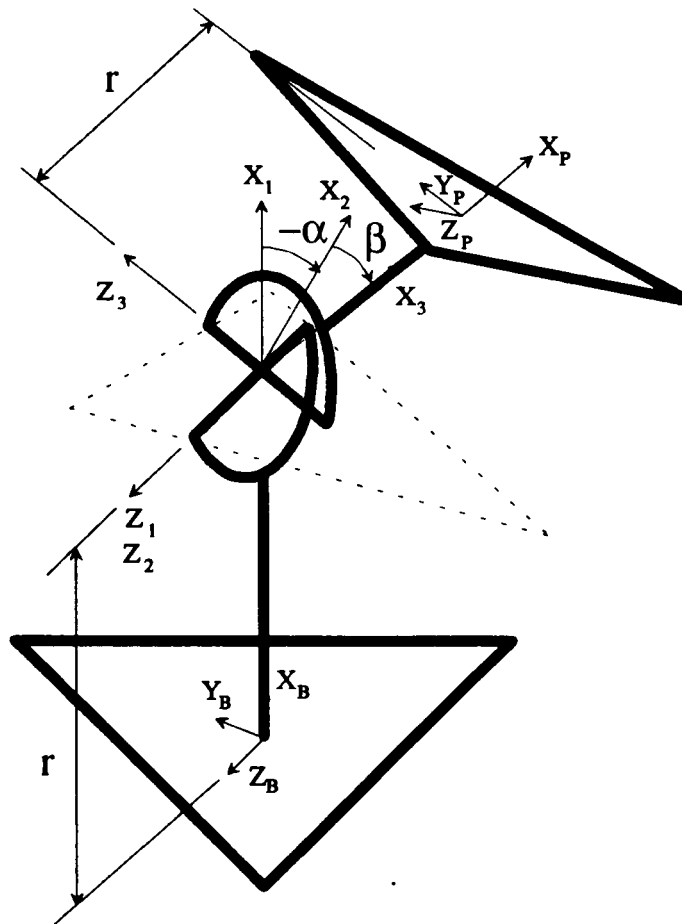
Figure D.1 Extensible Gimbal Kinematic Details

36

APPENDIX E.
VGT Node Locations

Following either the VGT forward or inverse kinematic position solution, the VGT node locations can be calculated. These node locations are required for finite element analysis and VGT graphical simulation. Figure E.1 shows the 12 VGT nodes calculated in this appendix. There are four sets of nodes: base nodes B_i, lower actuation plane nodes Q_i, upper actuation plane nodes Q_{iR}, and top platform nodes B_{iR} ($i = 1,2,3$) respectively. In this appendix these nodes are calculated given $\theta_1, \theta_2, \theta_3$, $\hat{U}_1$, α, β, r. All nodes are expressed with respect to the fixed {B} frame.
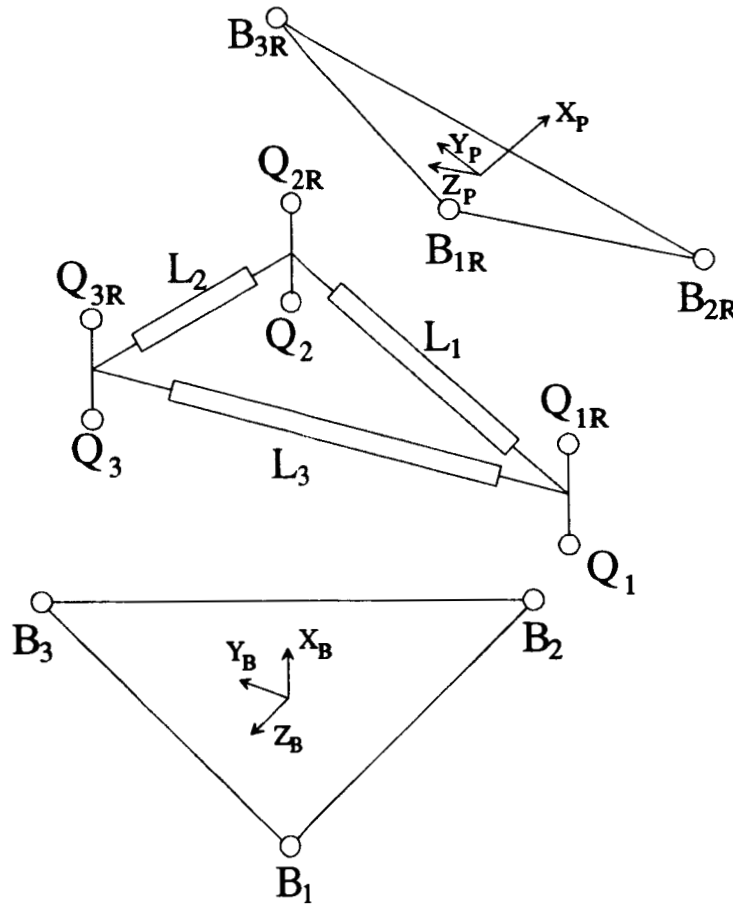
Figure E.1
VGT Node Locations

E.1 Base nodes $B_i; i = 1,2,3$

These are fixed for a single VGT cell. The geometry is shown in Fig. B.1.

$$^{B}B_1 = \left\{ \begin{array}{c} 0 \\ -L_0 \\ \dfrac{-L_0}{2\sqrt{3}} \\ \dfrac{L_0}{2} \end{array} \right\} \qquad ^{B}B_2 = \left\{ \begin{array}{c} 0 \\ -L_0 \\ \dfrac{-L_0}{2\sqrt{3}} \\ \dfrac{-L_0}{2} \end{array} \right\} \qquad ^{B}B_3 = \left\{ \begin{array}{c} 0 \\ \dfrac{L_0}{\sqrt{3}} \\ 0 \end{array} \right\} \qquad (E.1)$$

E.2 Lower actuation plane nodes $Q_i; i = 1,2,3$

These expressions were required for the VGT Forward A and VGT Inverse A solutions in Sections 4.1.1 and 4.2.1, respectively. Equation 5 is repeated in Eq. E.2. Appendix B presents fixed VGT geometric values used to calculate these nodes.

$$^{B}Q_1 = \left\{ \begin{array}{c} Ns_1 \\ O_{1y} + Nc_1 \\ 0 \end{array} \right\}, \; ^{B}Q_2 = \left\{ \begin{array}{c} Ns_2 \\ O_{2y} - \dfrac{N}{2}c_2 \\ O_{2z} + \dfrac{\sqrt{3}N}{2}c_2 \end{array} \right\}, \; ^{B}Q_3 = \left\{ \begin{array}{c} Ns_3 \\ O_{3y} - \dfrac{N}{2}c_3 \\ O_{3z} - \dfrac{\sqrt{3}N}{2}c_3 \end{array} \right\} \qquad (E.2)$$

E.3 Upper actuation plane nodes $Q_{iR}; i = 1,2,3$

These three nodes are $Q_i; i = 1,2,3$ reflected about the actuation plane of symmetry. They are calculated by extending the VGT joint offset along the actuation plane normal $\hat{U}_1$.

$$^{B}Q_{iR} = {}^{B}Q_i + S\hat{U}_1 \qquad (E.3)$$

E.4 Top platform nodes $B_{iR}; i = 1,2,3$

These three nodes are $B_i; i = 1,2,3$ reflected about the actuation plane of symmetry. They are calculated by transforming the top platform nodes from the {P} frame to the {B} frame.

$$^{B}B_{iR} = {}^{B}_{P}T \, {}^{P}B_{iR} \qquad (E.4)$$

38

The transformation matrix $^B_P T$, developed in Section 4.3.3, is repeated below.

$$\left[^B_P T \right] = \begin{bmatrix} c\alpha c\beta & -s\alpha & c\alpha s\beta & r(1+c\alpha c\beta) \\ s\alpha c\beta & c\alpha & s\alpha s\beta & rs\alpha c\beta \\ -s\beta & 0 & c\beta & -rs\beta \\ 0 & 0 & 0 & 1 \end{bmatrix} \qquad (E.5)$$

From symmetry, the top platform nodes in the $\{P\}$ frame are identical to the base nodes in the $\{B\}$ frame (see Figs. B.1 and B.2).

$$^P B_{iR} = {}^B B_i \qquad (E.6)$$

39

REPORT DOCUMENTATION PAGE

Public reporting burden for this collection of information is estimated to average 1 hour per response, including the time for reviewing instructions, searching existing data sources, gathering and maintaining the data needed, and completing and reviewing the collection of information. Send comments regarding this burden estimate or any other aspect of this collection of information, including suggestions for reducing this burden, to Washington Headquarters Services, Directorate for Information Operations and Reports, 1215 Jefferson Davis Highway, Suite 1204, Arlington, VA 22202-4302, and to the Office of Management and Budget, Paperwork Reduction Project (0704-0188), Washington, DC 20503.

1. AGENCY USE ONLY (Leave blank)	2. REPORT DATE May 1994	3. REPORT TYPE AND DATES COVERED Technical Memorandum

4. TITLE AND SUBTITLE
Kinematic Modeling of a Double Octahedral Variable Geometry Truss (VGT) as an Extensible Gimbal

5. FUNDING NUMBERS
233-03-03-02

6. AUTHOR(S)
Robert L. Williams II

7. PERFORMING ORGANIZATION NAME(S) AND ADDRESS(ES)
NASA Langley Research Center
Hampton, Virginia 23681-0001

8. PERFORMING ORGANIZATION REPORT NUMBER

9. SPONSORING / MONITORING AGENCY NAME(S) AND ADDRESS(ES)
National Aeronautics and Space Administration
Washington, D.C. 20546-0001

10. SPONSORING / MONITORING AGENCY REPORT NUMBER
NASA TM-109127

11. SUPPLEMENTARY NOTES

12a. DISTRIBUTION / AVAILABILITY STATEMENT
Unclassified - Unlimited
Subject Category - 63

12b. DISTRIBUTION CODE

13. ABSTRACT (Maximum 200 words)
This paper presents the complete forward and inverse kinematics solutions for control of the three degree-of-freedom (DOF) double octahedral variable geometry truss (VGT) module as an extensible gimbal. A VGT is a truss structure partially comprised of linearly actuated members. A VGT can be used as joints in a large, lightweight, high load-bearing manipulator for earth- and space-based remote operations, plus industrial applications. The results have been used to control the NASA VGT hardware as an extensible gimbal, demonstrating the capability of this device to be a joint in a VGT-based manipulator. This work is an integral part of a VGT-based manipulator design, simulation, and control tool.

14. SUBJECT TERMS
Degree-of-Freedom (DOF); Variable Geometry Truss (VGT); Extensible Gimbal; and In-Parallel Actuated Devices

15. NUMBER OF PAGES
40

16. PRICE CODE
A03

17. SECURITY CLASSIFICATION OF REPORT	18. SECURITY CLASSIFICATION OF THIS PAGE	19. SECURITY CLASSIFICATION OF ABSTRACT	20. LIMITATION OF ABSTRACT
Unclassified	Unclassified	Unclassified	UL